IEEE Open Journal of the
Industrial Electronics Society

Received 13 September 2023; revised 23 October 2023 and 9 November 2023; accepted 14 November 2023. Date of publication 29 November 2023;
date of current version 18 December 2023. The review of this paper was arranged by Associate Editor Binbin Li.

Digital Object Identifier 10.1109/OJIES.2023.3336981

DC Powering Solutions for the Future Circular Collider: Converter Topologies, Protection, and Control

MANUEL COLMENERO [1] (Student Member, IEEE), FRANCISCO RAFAEL BLANQUEZ [1] (Member, IEEE), AND RAMON BLASCO-GIMENEZ [2] (Senior Member, IEEE)

[1]CERN—European Organization for Nuclear Research, 1217 Meyrin, Switzerland
[2]Automatics and Industrial Informatics Research Institute, Universitat Politecnica de Valencia, 46022 Valencia, Spain

CORRESPONDING AUTHOR: MANUEL COLMENERO (e-mail: mcolmene@cern.ch)

ABSTRACT The future circular collider (FCC) is a cutting-edge particle accelerator being planned by the European Organization for Nuclear Research (CERN). It is designed to delve deeper into the mysteries of the universe than its predecessor, the large hadron collider (LHC). With a circumference of over 80 km, the FCC requires a reliable and efficient power transmission network to operate smoothly. The available power options for the FCC include a high-voltage dc transmission and radio frequency powering networks based on HVdc converters, such as the modular multilevel power converters or the 12-pulse thyristor rectifiers, each providing several benefits in power transmission efficiency and cost-effectiveness. However, the converter selection, its control, and the protection aspects must be carefully designed to meet the unique requirements of the installation. This article examines different dc powering scenarios for the FCC and proposes a control and protection scheme compatible with the accelerator's operation mode. This approach ensures that the power system meets the FCC's specific needs and operates safely and effectively. The validity of the proposed control and protection strategies is verified by means of detailed computer simulations.

INDEX TERMS HVdc power converters, power distribution control, power distribution faults, power electronics, reliability, voltage-source converters.

I. INTRODUCTION

The European Organization for Nuclear Research (CERN) is currently analyzing the feasibility of constructing a new large-scale particle accelerator, the future circular collider (FCC), with a circumference of 80–90 km [1]. The power required for the FCC's operation is projected to be around 400 MW. Thus, securing an efficient and robust power supply solution is essential to ensure the feasibility of the accelerator.

HVdc transmission could offer several advantages over conventional ac networks. In terms of transmission efficiency, a multiterminal dc (MTDC) network does not suffer from reactive power losses that are present in ac transmission systems [2] and compensation equipment [3] is no longer required. Additionally, there are no skin or proximity effects in cables, which further contribute to reducing losses [4]. Furthermore, dc cables have a higher transfer power capability compared to ac cables of the same size [5], making them more suitable for use in the FCC, where the cables must run along an already space-constrained accelerator tunnel.

Another advantage of HVdc is that it allows for precise control of the power flows. The FCC, which will be constructed along the French and Swiss borders, will receive its supply from cross-border transmission nodes of the 400 kV European Transport Network. Thus, it is important to ensure that the FCC does not interfere with the power flows established by network authorities and prevent uncontrolled power flows from being established through the FCC infrastructure. In this regard, the ac–dc converters can enhance network stability by precisely controlling the power flows [6] and injecting reactive power [7] into the connection nodes, thereby mitigating potential perturbations caused by the operation of the machine. Additionally, an HVdc network can compensate

voltage dips coming from the network [8]. These features can be easily accomplished by using modular multilevel converters (MMCs) [9], [10]. In terms of reliability, MMCs can ride-through a failure of one of its components by bypassing a faulty submodule [11], making it suitable for this application.

Regardless of the transmission scheme employed, the FCC will necessitate a significant fleet of high-power, high-voltage ac–dc converters to cater to one of the primary accelerator loads: the radio frequency (RF) system. Indeed, one of the main distinctions between a conventional HVdc network and the FCC is the need to accommodate the specific requirements of the RF system in terms of control and operation. In this context, the converters designated for the RF system must provide a set of RF amplifiers (klystrons) with dc voltages reaching up to 75 kV and an estimated power ranging from 150 to 200 MW. Given this, it is beneficial to explore solutions that could power both the RF system and the HVdc network. One possibility is using the same converter to serve both the RF and the dc network. Alternatively, other ac–dc converter topologies, such as line-commutated converters (*LCC*) [12], can be paired with voltage-source converters for reactive power and harmonic compensation [13]. These converters demand specialized control design methods to meet the RF power demand requirements.

Protection is another crucial aspect to consider when using a dc network. In comparison to a conventional ac network, dc short-circuits require more complex protection strategies due to the absence of current zero-crossing in dc and the increased susceptibility of converters to fault transients. Here, there are also significant differences between the FCC and a conventional HVdc network. Due to the high-electric fields used in klystrons, internal arcing can happen with relatively high frequency [14], leading to dc short-circuits more often than in conventional HVdc links. Under the scenario considered, where the klystrons share a common dc bus, this fault must be cleared very quickly to avoid damaging the sensitive RF equipment. Therefore, protecting the RF system is particularly challenging.

Accordingly, this article presents the use of HVdc networks for powering accelerator equipment and RF loads. It explores various dc powering scenarios and proposes technical solutions for supplying both the RF and transmission networks. As part of these solutions, the employment of three-terminal MMCs is introduced, and its control method, which is based on the injection of circulating currents, is further discussed. Although the MMC with several terminals has been analyzed in other publications [15] for transmission, its use when supplying an RF load and the specificities of its control require further study. Additionally, this article delves into the protection of the system across the different scenarios considered and suggests a sequence for clearing a dc fault and restoring the system. The recommended solutions and control methods have been simulated using MATLAB/Simulink.

The rest of this article is organized as follows. The first section briefly outlines the control and protection requirements for both the transmission and RF networks. The subsequent section introduces the proposed dc powering scenarios. The following section delves into the converter topologies and their control, with a focus on the three-terminal MMC. Finally, various protection strategies are presented and assessed through detailed simulations. This analysis offers insights into the primary constraints of the systems and suggests feasible solutions for consideration in the subsequent phases of the FCC design.

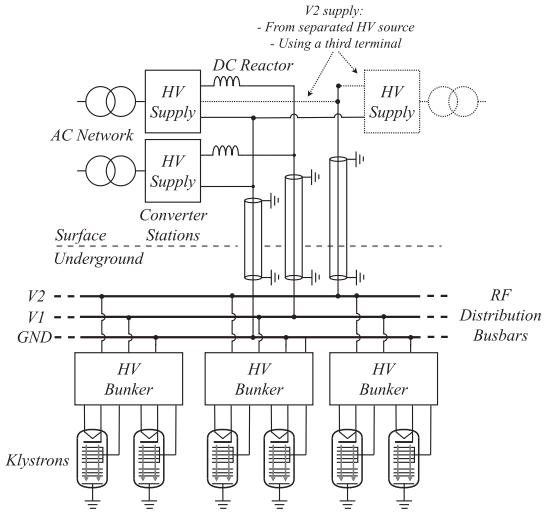

FIGURE 1. Architecture of the RF network. Several rectifiers can be connected in parallel for redundancy. The V1 voltage can be created using a low-power supply or the third terminal of the MMC (Scenario III).

II. CONTROL AND PROTECTION REQUIREMENTS

The FCC will require to supply three-terminal klystrons [16] connected to a common dc busbar supplied by one or more surface power converters. The most recent concept for the FCC klystrons will use two series-connected voltage supplies, rated at 60 and 12 kV, to supply the middle and top terminals, respectively (the bottom terminal is connected to ground), as shown in Fig. 1. The 60 kV supply is fixed (denoted as $V1$ in Fig. 2), while the 12 kV supply must be adjustable to regulate the RF power. During normal operation, the middle terminal of the klystron absorbs a negligible current, so the top and bottom terminals are used to supply bulk power to the klystron via the 72 kV voltage supply (denoted as $V2$ in Fig. 2). Therefore, the supply must be capable of regulating its voltage between 60 and 72 kV. The power in this configuration follows a nonlinear relation, starting at values close to zero for 60 kV and reaching the nominal value for 72 kV [17]. The $V1$ and $V2$ voltage can be generated by using two independent voltage supplies or a converter with three dc terminals.

If the klystrons are supplied from the main dc busbar, then it is not possible to individually control RF power deviations, which is usually desired. To cope with this issue, trimming converters connected in series with groups of klystrons can be added. These converters can supply or absorb a certain

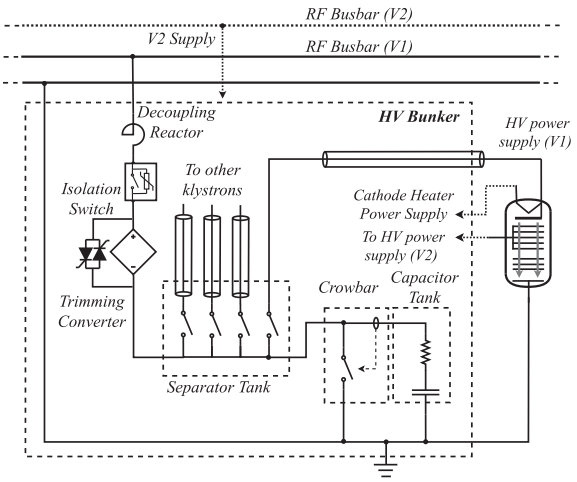

FIGURE 2. Schematic diagram of an RF bunker. The separator tank allows us to connect/disconnect the individual. The capacitor tank filters out the dc voltages across klystron terminals. The trimming converter is used for fine tuning of the klystron voltages. The decoupling coil allows us to limit the fault current in case of fault.

amount of power to correct small power deviations. Decoupling control avoids interactions between converters [18]. These converters can be bypassed in case of fault using antiparallel thyristors [19] (see Fig. 2).

Regarding RF protection, it is essential to provide fast-acting protection elements to prevent the energy stored by cables and filtering elements from discharging into the klystron in the event of a fault, given that the maximum energies that can be discharged into the klystron are extremely low (around 20–30 J for commercial klystrons [20]).

A widely used technique for protecting klystron tubes from arcing in RF systems is to activate a crowbar mechanism when an arcing fault is detected [21]. This crowbar is designed to quickly short circuit the energy stored in the cable and in the filtering elements of the system so that it does not flow into the klystron (see Fig. 2). This is, for example, the approach followed in the case of the LHC [22].

When the crowbar is triggered, the klystron is protected, but a dc short-circuit is now created across the dc terminals. If no measures are taken, a significant amount of current might flow into the crowbar from the mains, potentially damaging it. To avoid this issue, fast interruption of the fault current must be achieved. Since dc voltage control is required, fault-blocking topologies can be used. These converters can immediately invert the polarity of their output voltages to de-energize the dc bus and avoid the crowbar overload.

Meanwhile, the operation of the MTDC network requires that one rectifier controls the dc voltage whereas the other regulates the power taken from the ac network. Other alternative control methods, such as droop control [23], can also be employed. In both cases, achieving optimal power flow involves appropriately configuring the set points for voltage and power in the first case, and droop curves in the other based on the operating conditions. The inverter stations responsible for supplying ac distribution networks at the access points act as constant power loads. To establish the access point networks in the absence of auxiliary supply, specific control techniques [24] are implemented.

In terms of protection of the MTDC, the main priority in the event of a fault is to limit the energy discharged, rather than quickly isolating the fault and restarting the system. The dc line runs along the accelerator tunnel, which makes it particularly vulnerable to short circuits that could potentially damage sensitive equipment. In this sense, the behavior of the dc network during a fault is highly dependent on the grounding scheme employed. In a bipolar configuration, a metallic return is necessary to operate with reduced power in the event of a contingency [25]. In this case, all faults will result in high-fault currents [26]. On the other hand, under a symmetric monopole configuration [27], only pole-to-pole faults will result in high overcurrents. In the event of a pole-to-ground fault, the fault current is significantly reduced due to the system's grounding through a high-value impedance [28]. However, the main drawback is the occurrence of an overvoltage on the healthy pole, which must be discharged within a short time to avoid damage, either using the converter [29] or by means of a discharge resistor [30]. On the other hand, if the RF and the transmission network are combined, an asymmetric monopolar configuration is needed since the RF system requires one pole to be grounded. For the case where the systems are independent, a symmetric monopolar configuration is preferred considering its lower cost [31].

It should be noted that since the access point networks are not connected to the ac network (or they are connected to a weak auxiliary network), the rectifier stations are the primary contributors to the fault current. Therefore, protection can be optimized by installing the primary fault current limiting devices only in those converters and relying on converter blocking in the others to avoid perturbation of access point networks.

III. OVERVIEW OF DC POWERING SCENARIOS

Taking into account the voltage and power requirements of the RF systems, the following three different dc powering scenarios have been considered.

1) Scenario I (see Fig. 3): RF system and the dc transmission network powered by separate power converters.
2) Scenario II (see Fig. 4): *LCC* are used to provide power to the RF system, while the converter supplying the dc network is also utilized to compensate for the reactive power and harmonics generated by the *LCC*.
3) Scenario III (see Fig. 5): The RF system shares a power converter with the dc network.

In all three scenarios, it is assumed that the FCC is powered from two connection points to the 400 kV network. Local acceleration equipment will be connected to medium voltage access point networks, which would be powered by conventional half-bridge MMCs connected to the main dc busbar.

Each of the three scenarios presents its own set of advantages and disadvantages. In Scenario I, the MMC converters

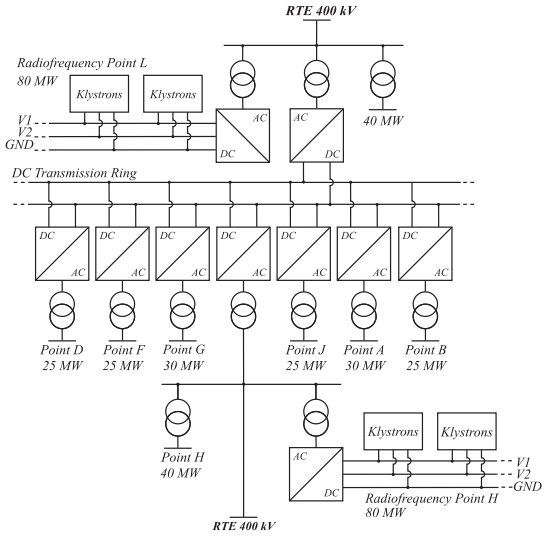

FIGURE 3. DC powering scenario I: Separate converters for RF and dc networks.

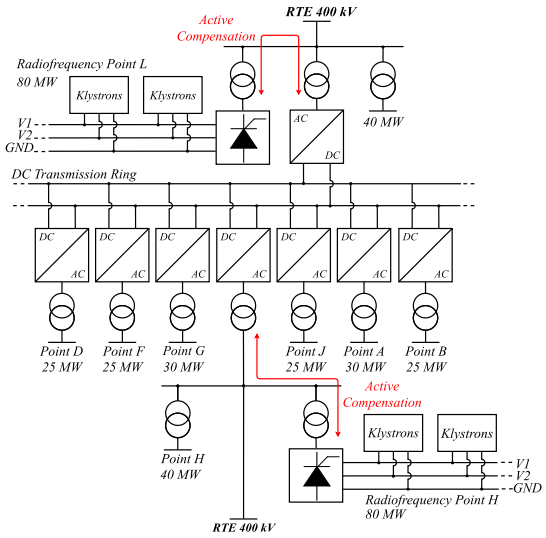

FIGURE 4. Scenario II: Powering the RF system with an *LCC* converter and active compensation with an MMC.

designated to power both the RF and the dc network function independently, promoting improved optimization and enhanced reliability. However, the absence of shared resources results in a higher overall cost and increased losses for this solution. Scenario II provides a compelling approach in terms of RF converter cost and efficiency. Thyristor converters are more cost-effective than MMCs, largely due to their fewer components. Furthermore, switching losses in this converter design are minimal, yielding a significant efficiency advantage over the MMC. However, these benefits are somewhat offset by the necessity to enlarge the MMC, leading to greater losses from active compensation. In Scenario III, there is a focus on efficient resource sharing, but it adds complexity to the network's operation, especially regarding control and protection. This scenario also constrains operational flexibility, as

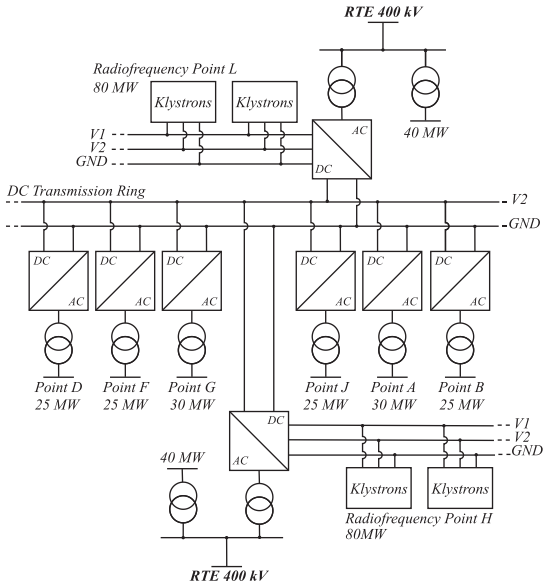

FIGURE 5. Scenario III: Powering the RF system and the dc network with a single power converter.

the converter must remain operational even when the RF is not in use. Table 1 summarizes the main differences among the three analyzed scenarios.

IV. CONVERTER TOPOLOGIES

This section includes a brief introduction of four candidate converter topologies for the FCC.

A. HALF-BRIDGE MMC

One option to supply the MTDC network and converters for the access points is through the use of the half-bridge MMC topology. This topology has been demonstrated to have lower costs and losses compared to other options [32]. However, it should be noted that in the event of a dc short-circuit, an external interrupting device must be added to clear the fault.

B. HYBRID MMC

The hybrid MMC topology has the ability to adjust its dc voltage within a specific range while maintaining high ac voltage [33]. To achieve this, a certain number of full-bridge cells need to be added. Consequently, this topology is a suitable option for supplying the RF system when a separate dc voltage source is used to power the V2 terminal. Additionally, by incorporating enough of these cells, the hybrid MMC topology can control the fault current [34]. The diagram of the converter is shown in Fig. 6.

C. ACTIVELY-COMPENSATED THYRISTOR RECTIFIER

A potential way to enhance the powering scheme is to utilize thyristor rectifiers as the converters for supplying the RF system ($V1$). Compared to MMCs, thyristor rectifiers have the advantages of lower losses, lower volume, reduced complexity, and greater robustness [35]. Additionally, in case of a dc fault, they can limit the fault current by forcing the station

TABLE 1. Comparison Between DC Powering Scenarios

Scenario		Comparison
I	×	High cost: Two full MMCs are required. The surface required by the RF rectifier is larger than in Scenarios II and III.
	✓	Simplified protection: Klystron arcing does not impact the dc network.
	✓	Simplified control: RF voltage is controlled independently.
	×	Higher losses: Losses in Scenario I are higher than in II and III.
II	✓	Low RF cost: Lower cost of the thyristor converter compared with the MMC.
	×	Higher MMC cost: Needs to be overdimensioned for compensation.
	✓	Simplified protection: Independent protection schemes for transmission and RF. The thyristor converter can block dc faults.
	✓	Simplified Control: RF voltage is controlled independently.
	✓	Lower RF losses: Losses in the thyristor converter are lower than in an MMC equipped with full-bridge submodules.
	×	Higher MMC losses: Due to reactive power and harmonic compensation.
III	✓	Low cost: Footprint is minimized compared with Scenarios I and II.
	×	Complex protection: RF faults are seen by the dc network and vice versa.
	×	Complex RF Operation: Ramping up of dc voltage is not possible.
	×	Complex control: DC voltage depends on RF operation (within a margin).
	✓	Lower losses: Main components are used for the simultaneous supply of RF and dc network.

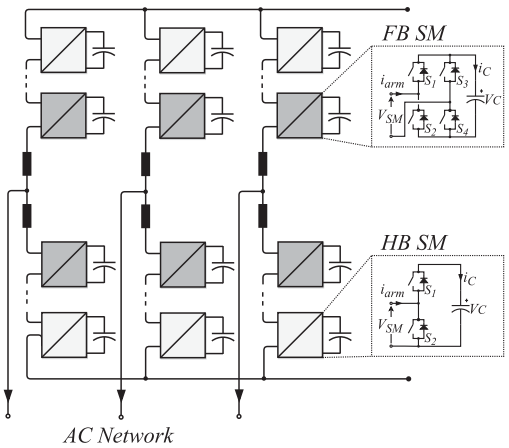

FIGURE 6. Schematic representation of a hybrid MMC. The number of full-bridge submodules is selected based on the minimum dc voltage required.

into inversion mode [36]. However, during operation, thyristor converters absorb a significant amount of reactive power and generate harmonics that could disrupt the network [37].

To cope with this issue, the MMC converter used to supply the MTDC network can also perform the task of compensating

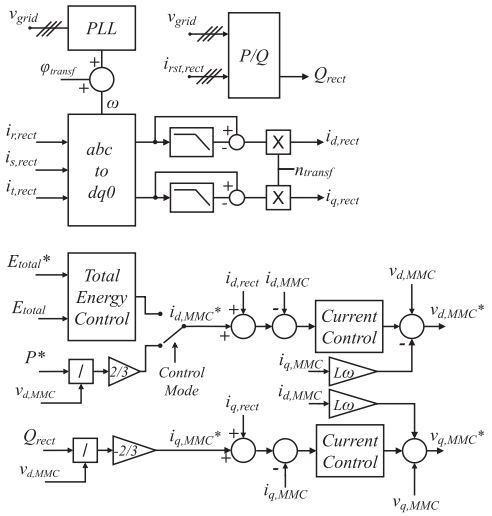

FIGURE 7. Modification of the MMC grid current controller when it is used as an active filter. The grid voltages and currents at the 400 kV busbar are used as measurements for compensation. Therefore, the shift and amplitude changes introduced by the transformers must be taken into account (φ_{transfo} and n_{transfo}). The current control is implemented using PIR controllers.

the reactive power and the harmonics generated by the RF rectifier. This can be done by modifying its control according to the diagram shown in Fig. 7. The measurement of the reactive power Q_{rect} is used to set the reference for the q-frame current, $i^*_{q,\text{MMC}}$. The high-frequency components of the thyristor converter current are obtained in the dq-frame ($i_{d,\text{rect}}, i_{q,\text{rect}}$) and injected into the MMC current control. Note that the amplitude and phase change introduced by the transformer need to be taken into account for this. Since harmonics will appear as sinusoidal references in the synchronous reference frame, resonant regulators are added for their proper tracking and compensation.

D. THREE-TERMINAL MMC

To minimize the footprint of the powering system, an additional terminal can be incorporated into the MMC for either providing the $V2$ voltage in scenario I or for simultaneously powering the RF and MTDC network in scenario III. If a three-terminal MMC is used for powering the RF under scenario I, the middle terminal of the MMC will supply a negligible current to the RF system ($I_2 \approx 0$). However, in scenario III, the third terminal will deliver a substantial amount of current to the dc network.

In both scenarios, directly connecting the three phases of the MMC via the tapping point is unfeasible without the use of an ac filter. This filter can either be realized using submodules for electronic filtering or by incorporating a reactor with high ac impedance. Given the necessity for controllability, the first option is chosen. Consequently, adding extra reactors to both the top and middle arms becomes necessary to isolate their dynamics. The inductance, determined by methods documented in the literature [38], is allocated between the upper and lower

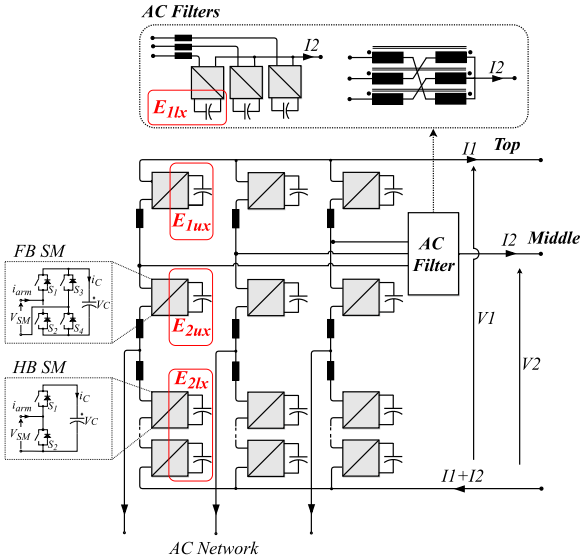

FIGURE 8. Schematic diagram of the three terminal MMC. The use of submodules or a reactor with high ac impedance is necessary to implement the ac filter and prevent the flow of ac currents into the dc network. The notation for the energies of the converter arms is shown in red.

arms so that the inductance perceived from the ac network remains consistent between the two. The distribution of inductance within the upper arms is then proportioned based on the ac voltage distribution.

A diagram of the converter showing the three-terminal connection is shown in Fig. 8.

Focusing on Scenario III, the converter must be able to operate reliably under several conditions. During normal operation, the converter controls the $V2$ voltage to a fixed reference determined by the RF requirements and changes the $V1$ according to the RF system demand. In this case, the $V2$ voltage is fixed by the RF requirements but used as a controlled voltage for the MTDC. Conversely, during fault conditions, the converter should be capable of operating with low dc voltages, nearing zero for low-impedance faults.

The main challenge of this converter is controlling the internal arm energies due to the flow of asymmetric dc currents through the converter arms. In a conventional MMC, the ac power absorbed from the ac side is compensated by the dc power supplied to the dc network. However, in the case of the three-terminal MMC, this compensation is no longer possible, and the ac and dc arm powers become imbalanced. Furthermore, this imbalance changes from one operation mode to another. Therefore, an alternative control strategy is required.

The proposed control strategy for the three-terminal MMC can be summarized as follows: The converter is formed by 12 arms, and the energies of these arms need to be controlled. These energies can be expressed as the energy differences between upper and lower arms (vertical balancing) and the energy differences between the arms belonging to different phases (horizontal balancing). The following definitions

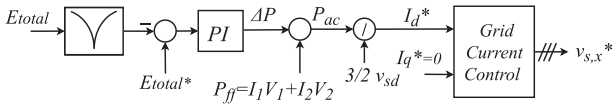

FIGURE 9. Converter total energy control. The converter controls the dc voltage.

are required: the energy differences between the two upper and the lower arm of the main MMC branch for phase x (E_{1ux}, E_{2ux}, and E_{2lx}, respectively) are denoted as $E_{t,x}$, and the energy difference between the two upper arms of the main branch for phase x (E_{1ux}, E_{2ux}, respectively) is denoted as $E_{m,x}$. The energy of the three main arms that compose the MMC main branch (E_{1ux}, E_{2ux}, and E_{2lx}) for phase x are denoted as E_x^{Σ}. The following expressions are used to calculate these components

$$E_{t,x}^{\Delta} = E_{1ux} + E_{2ux} - E_{2lx} \tag{1}$$

$$E_{m,x}^{\Delta} = E_{1ux} - E_{2ux} \tag{2}$$

$$E_x^{\Sigma} = E_{1ux} + E_{2ux} + E_{2lx}. \tag{3}$$

To fully define the controlled energies, three more degrees of freedom must be determined. The energies of the middle-terminal branches are selected as the independent control variables, as given by (4)

$$E_{1lr} = E_{1ls} = E_{1lt} = E_{1l,\text{rated}}. \tag{4}$$

Furthermore, the total energy stored in the MMC, E_{total}, is utilized as a controlled variable, as shown in (5)

$$E_{\text{total}} = \sum_{x=r,s,t} E_{1ux} + E_{1lx} + E_{2ux} + E_{2lx} \tag{5}$$

After determining the controlled variables, an appropriate control structure can be selected. However, the conventional method of managing arm energies by injecting ac currents that are in phase with the network voltage and distributing the dc current between converter arms is insufficient for three-terminal MMCs. Therefore, the proposed solution involves injecting a second circulating current at a frequency of 100 Hz, which is different from that of the mains. This current is in phase with a 100 Hz voltage source generated by the arms whose energy is being controlled. Moreover, the positive and negative sequences of this current can be managed, providing additional degrees of freedom. The 50 Hz currents are also employed for internal power transfer.

In the case of a three-terminal MMC, the control process involves multiple energy control loops, where the total energy control loop is the highest level. The MMC regulates the overall energy stored within the converter via the ac current reference, while the total dc power serves as a feed-forward signal. Since energy control focuses on the average values of the energies, notch filters tuned at ω_g and $2\omega_g$ are employed to calculate controlled energies. The total energy controller is shown in Fig. 9.

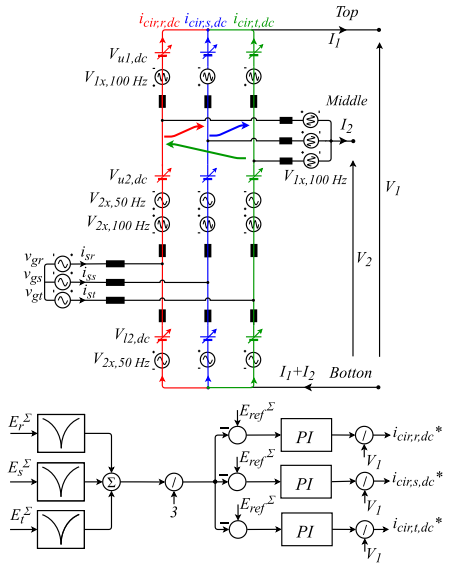

FIGURE 10. Operation principle and schematic of the horizontal balancing controller.

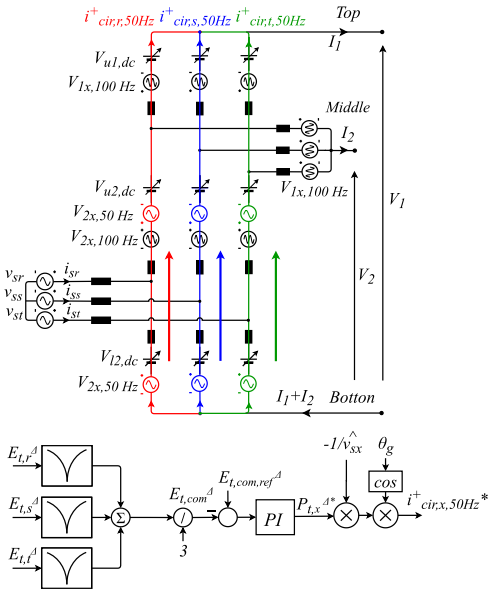

FIGURE 11. Operation principle and schematic of the vertical balancing controller. in this case, the difference between the energies of upper and lower arms is controlled using the positive sequence of the 50 Hz circulating current.

The control scheme for horizontal balancing of the main arms' energies in the MMC involves controlling the sharing of the dc components of the circulating currents, $i_{cir,x,dc}$. The dc current path and the equivalent voltage sources involved in this process are depicted in Fig. 10. Power is transferred when the dc current flows through the equivalent dc source created by the arm, thus achieving horizontal energy balancing.

To balance the energy differences between the upper and lower common arms in the MMC, the positive and negative sequences of the 50 Hz circulating current are controlled. The positive sequence controls the energy difference between the three upper and lower arms, as shown in Fig. 11. The angle of the network, θ_g, determines the phase of the circulating current. Conversely, the differences between the differential energies of the arms belonging to different phases are controlled through the negative sequence, as depicted in Fig. 12. The amplitude of the negative-sequence circulating currents at 50 Hz is calculated in the *dq*-reference frame using the following expression:

$$i^{\Delta *}_{cir,d,50\ \mathrm{Hz}} + j \cdot i^{\Delta *}_{cir,q,50\ \mathrm{Hz}} = \frac{P^{\Delta *}_{td} + j \cdot P^{\Delta *}_{tq}}{-V_{2x,50\ \mathrm{Hz}}} e^{j(\omega_g t)} \qquad (6)$$

To establish control of $E^{\Delta}_{m,x}$ and E_{1lx}, the positive and negative sequences of the 100 Hz circulating current can be utilized, as illustrated in Figs. 13 and 14. In the former case, the controller sets the reference for the circulating current flowing through the main arms, while in the latter case, it is the current flowing through the middle-terminal arms that is controlled. The negative sequence of the circulating current is calculated using the following expressions in these cases:

$$i^{\Delta *}_{cir,2d,100\ \mathrm{Hz}} + j \cdot i^{\Delta *}_{cir,2q,100\ \mathrm{Hz}} = \frac{P^{\Delta *}_{md} + j \cdot P^{\Delta *}_{mq}}{-V_{2x,100\ \mathrm{Hz}}} e^{j(2\omega_g t)} \qquad (7)$$

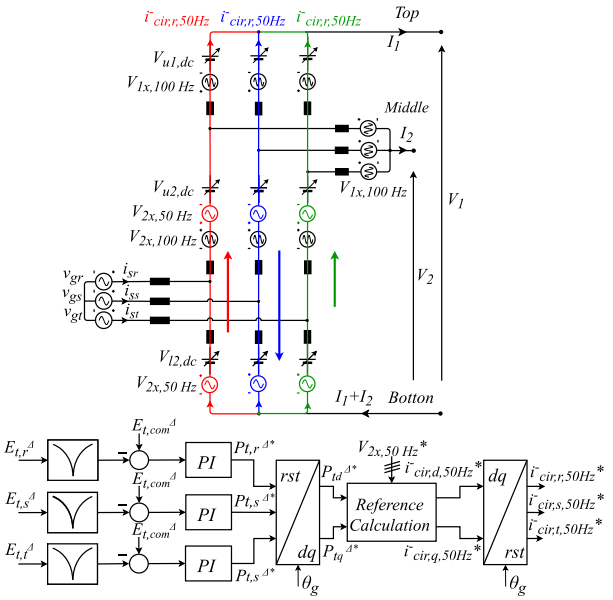

FIGURE 12. Operation principle and schematic of the vertical balancing controller. In this case, the difference between the energies of the upper and lower arms belonging to different legs is controlled using the negative sequence of the 50 Hz circulating current.

$$i^{\Delta *}_{cir,1d,100\ \mathrm{Hz}} + j \cdot i^{\Delta *}_{cir,1q,100\ \mathrm{Hz}} = \frac{P^{\Delta *}_{1d} + j \cdot P^{\Delta *}_{1q}}{-V_{1x,100\ \mathrm{Hz}}} e^{j(2\omega_g t)}. \qquad (8)$$

The control diagram depicted in Fig. 15 is utilized to accurately track the circulating current references. To track the sinusoidal references, proportional-resonant control is employed. The dc and ac components of the circulating currents

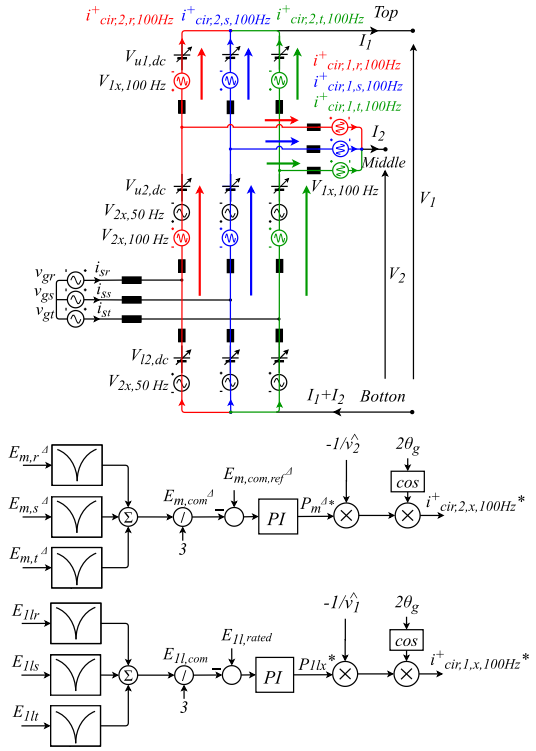

FIGURE 13. Vertical balancing of the common energies of the upper arms and the middle branch. In the first case, the difference between the energies of the common branch are controlled using the positive sequence of the 100 Hz circulating current. In the second case, 100 Hz currents of positive sequence are injected into the middle branch.

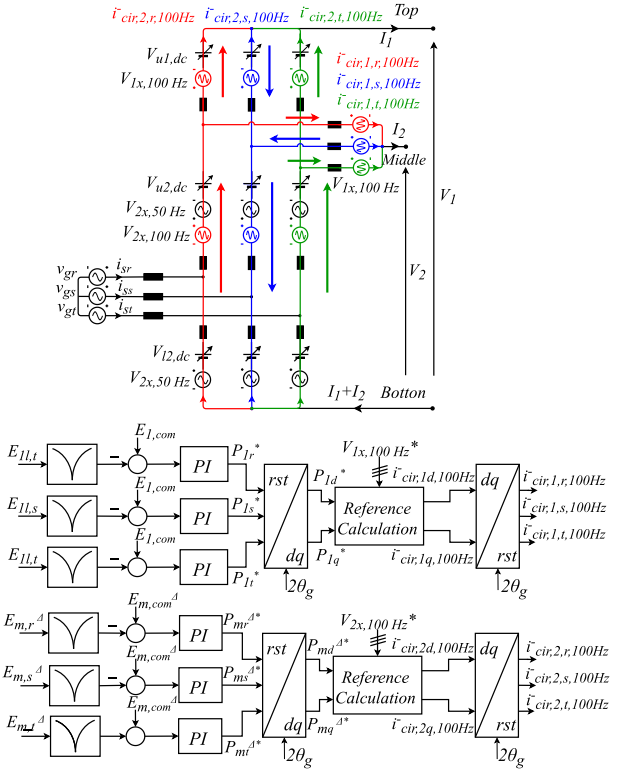

FIGURE 14. Vertical balancing of the differential energies of the upper arms and the middle branch. In the first case, the difference between the energies of the common branch are controlled using the negative sequence of the 100 Hz circulating current. In the second case, 100 Hz currents of negative sequence are injected into the middle branch.

are extracted using a notch filter and a bandpass filter. Apart from the circulating current control loop, the MMC control requires a dc voltage control loop to control the RF power, and a low-level control, which involves the pulsewidth modulation modulators and the submodule energy balancing. This last loop employs a conventional sorting algorithm modified for operation with full-bridge submodules to keep the cell voltages balanced.

To validate the proposed control strategy, a simulation of a three-terminal MMC was conducted. This model powers two loads: a 30 MW nonlinear load connecting the top and bottom terminals, and a 36 MW linear load linking the middle and bottom terminals. The converter draws power from a 40 kV ac network. Given the need for complete dc voltage control in this scenario, full-bridge submodules are utilized. The submodule capacitance is determined using a standard energy value of 40 kJ/MVA, and a submodule voltage of 1 kV is implemented. Full-bridge submodules are added to the arms considering the negative voltage generation needs. The simulation model comprehensively represents all submodules. Table 2 summarizes the main parameters of the converter used for simulation.

Fig. 16(a) shows the $V1$ and $V2$ voltages being ramped-up from zero. When the $V1$ voltage is increased, the linear load absorbs current. Nevertheless, the nonlinear one, representing

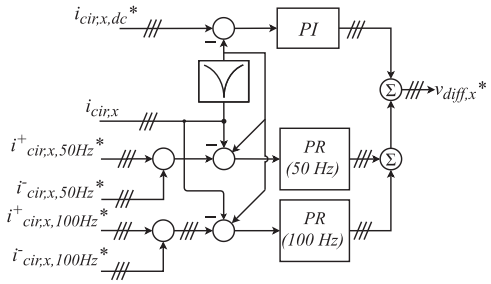

FIGURE 15. Circulating current control. This block is used to control the circulating current flowing through the main arms and the current flowing into the middle arms.

TABLE 2. Three-Terminal MMC Parameters Used in Simulation

Parameter	Value
Rated Power	100 MW
Rated middle dc voltage (V1)	60 kV
Rated upper dc voltage (V2)	72 kV
Rated ac voltage	40 kV
Rated energy	40 kJ/MVA
Submodule voltage	1 kV
Submodule capacitance	0.018F
Number of SM (upper subarms)	25 (10 FB)
Number of SM (lower subarms)	10 (10 FB)
Number of SM (upper arms)	50 (25 FB)
Number of SM (lower arms)	65 (30 FB)

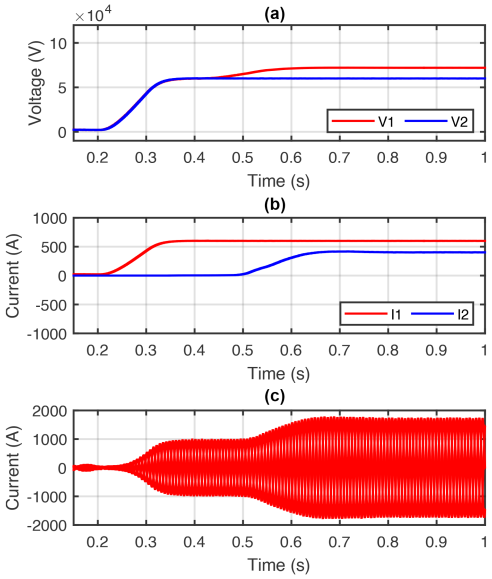

FIGURE 16. Input and output voltages and currents. (a) DC voltages. (b) DC currents. (c) AC currents.

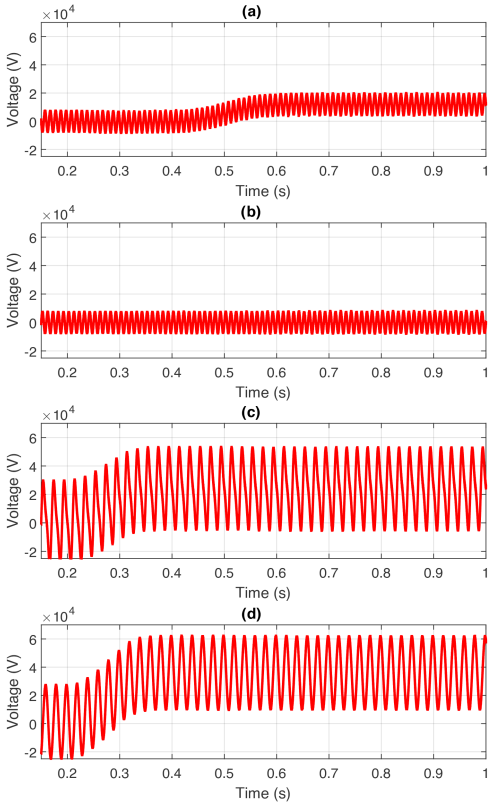

FIGURE 17. Voltages generated by the arms of phase R. (a) Upper subarms. (b) Lower subarms. (c) Upper arms. (d) Lower arms.

the behavior of the second stage of the RF system is still around zero. When the second stage starts to increase, then the nonlinear load starts to pull current from the converter [see Fig. 16(b)]. This is reflected in the ac currents absorbed by the converter [see Fig. 16(c)].

On the other hand, Fig. 17 shows the arm voltages generated by the converter. As mentioned, ac components are selected to transfer power between them using the 50 and 100 Hz components.

Finally, Fig. 18 shows the average submodule voltages. It can be observed that the submodule ripple is higher when the converter is operating at full power due to the circulation of harmonic currents used to balance the arms. As it can be seen, the proposed strategy is able to keep the arm energies controlled at various operation points.

V. PROTECTION

A. PROTECTION OF THE MTDC NETWORK UNDER SCENARIOS I AND II

Two protection philosophies have been proposed for scenarios I and II in the MTDC network. The first approach relies on ac breakers for fault clearance, while the second utilizes the hybrid MMC. In both scenarios, a symmetric monopole grounding scheme is employed.

In a network protected by ac breakers and half-bridge MMCs (see the circuit shown in Fig. 19), a pole-to-pole short circuit can cause an immediate blocking of the converters due to the discharge of submodule capacitors. However, since ac breakers have a typical operation delay of 30–60 ms, high-fault currents may still build up due to the contribution of the ac network. This can lead to significant energy storage in the system inductors that will discharge into the fault after isolation.

After the fault current has decayed to zero, the faulty line can be isolated using conventional switches. In the FCC network, this would require operating with the transmission ring open, which may result in the need to operate the accelerator in a degraded mode to avoid exceeding the limits on the remaining lines. Once the faulty line is isolated, the restoration sequence can be initiated.

The restoration process of the MTDC network involves a series of steps, such as energizing the network with ac preinsertion resistors, unblocking the rectifiers, ramping up the network voltage to its nominal value, and finally unblocking the inverters, as illustrated in Fig. 20. Adherence to this sequence is crucial for the safe and efficient restoration of the network. It is again worth noting that the inverter stations block when a fault is detected and do not contribute significantly to the fault current since they are connected to passive networks.

A pole-to-ground fault can be protected by a similar approach. The fault current in this case is much lower, especially if high impedance grounding is used. However, an overvoltage will still appear on the healthy pole after the fault, which can potentially overstress it despite the operation of surge arresters. To prevent this, the MTDC network is discharged

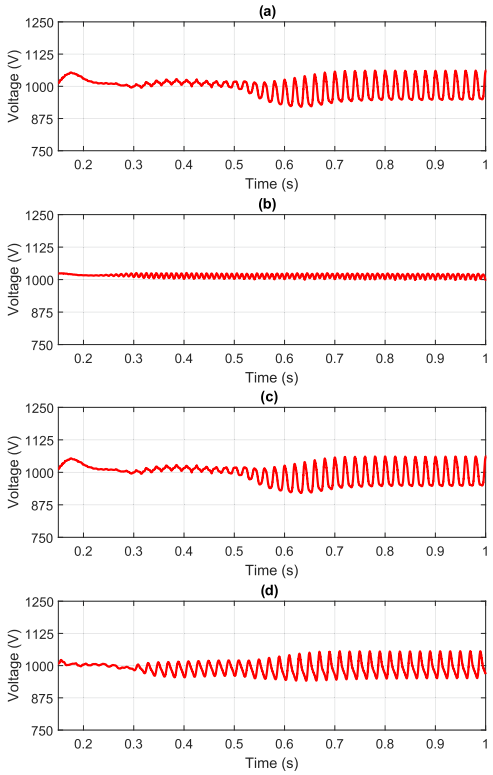

FIGURE 18. Average submodule voltages. (a) Upper subarms. (b) Lower subarms. (c) Upper arms. (d) Lower arms.

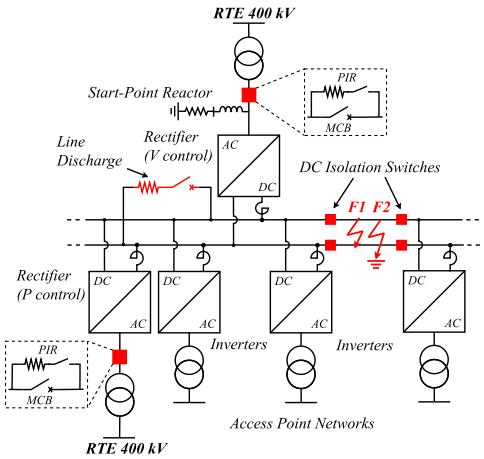

FIGURE 19. Circuit used to study protection based on ac breakers. F1 is a pole–pole short circuit whereas F2 is a short circuit to ground. The isolation switches are modeled as conventional ac breakers. Start-point reactor is used for grounding. Surge arresters are also considered.

using a resistor and then restarted, similar to the pole-to-pole fault case. The fault clearing sequence is depicted in Fig. 21.

On the other hand, the use of hybrid MMCs for the rectifier stations (see Fig. 22) can greatly reduce the magnitude of the fault current and, consequently, the energy discharged during a pole-to-pole fault. This is accomplished by immediately

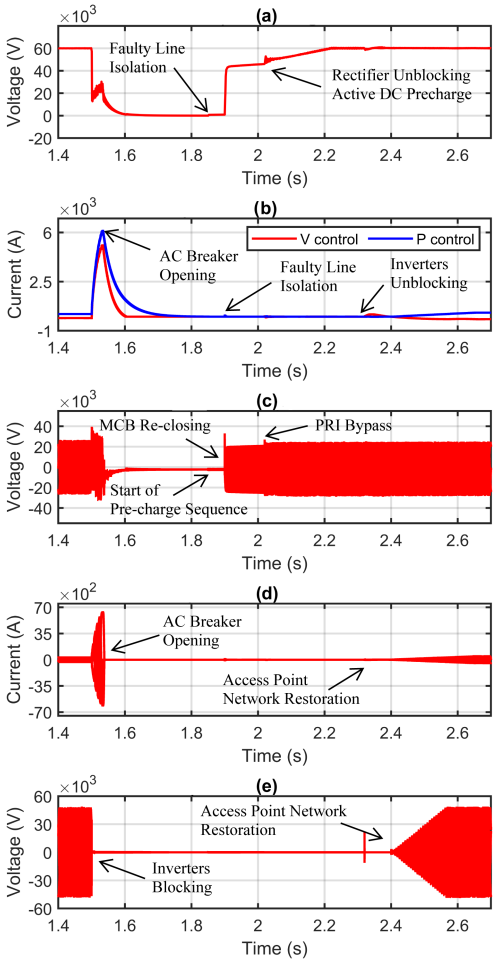

FIGURE 20. Pole-to-pole protection sequence when using ac breakers. (a) DC voltage measured at the rectifier terminals. (b) DC current measured at the rectifier terminals. (c) AC voltage of the rectifier stations. (d) AC current of one of the rectifier stations. (e) Voltage at one of the medium voltage access point networks.

reducing or reversing the polarity of the dc voltage upon detecting the fault. Since less energy is transferred to the system inductance, faster isolation is possible, and damage at the fault location can be minimized. Additionally, the converter itself can restore the dc voltage, resulting in a faster restoration process without the need for preinsertion resistors. The protection sequence for a pole-to-pole fault is shown in Fig. 23.

In the case of a pole-to-ground fault, the network is de-energized by bringing the dc voltage to zero in a controlled way, thereby preventing overvoltage caused by the fault and reducing stress on surge arresters, cables, and transformers. The network can then be restored as in the previous case. The protection sequence for this scenario is illustrated in Fig. 24.

B. PROTECTION OF THE RF NETWORK UNDER SCENARIOS I AND II

The RF network is protected by rapidly inverting the dc voltage as soon as a fault is detected. Unlike the MTDC network,

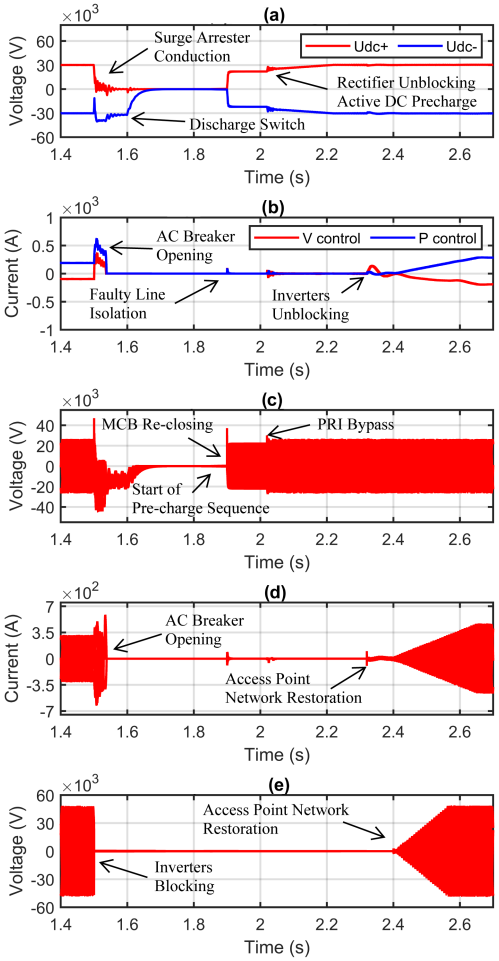

FIGURE 21. Pole-to-ground protection sequence when using ac breakers. (a) DC voltage measured at the rectifier terminals. (b) DC current measured at the rectifier terminals. (c) AC voltage of the rectifier stations. (d) AC current of one of the rectifier stations. (e) Voltage at one of the medium voltage access point networks.

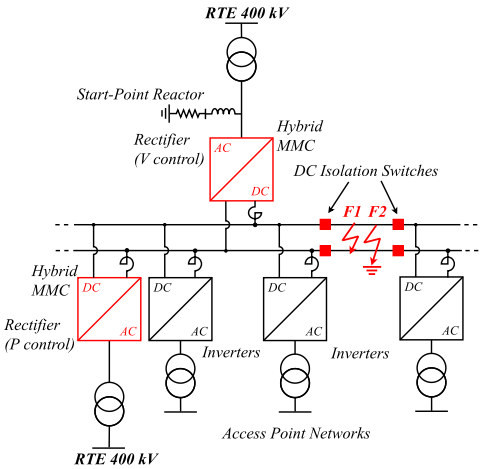

FIGURE 22. Circuit used to study protection when hybrid rectifiers are used. F1 is again a pole–pole short circuit whereas F2 is a short circuit to ground. Surge arresters are also considered.

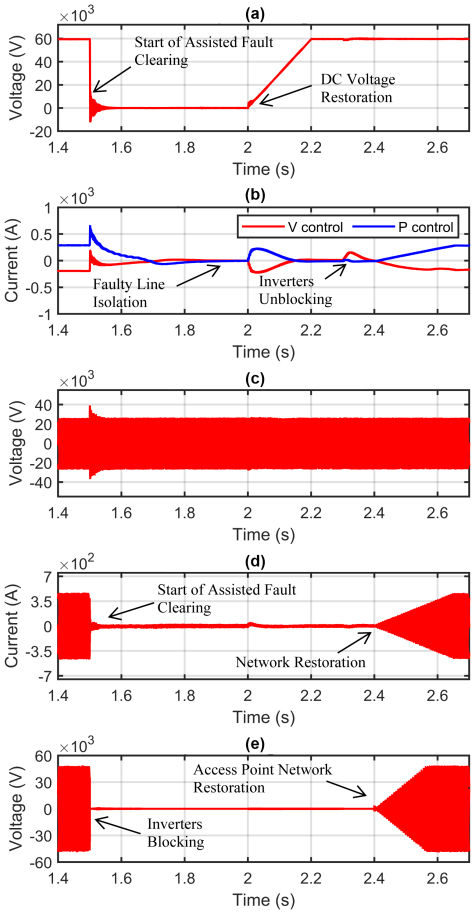

FIGURE 23. Pole-to-pole protection sequence when using hybrid converters. (a) DC voltage measured at the rectifier terminals. (b) DC current measured at the rectifier terminals. (c) AC voltage of the rectifier stations. (d) AC current of one of the rectifier stations. (e) Voltage at one of the medium voltage access point networks.

the priority for the RF system is to de-energize the energy stored in the filtering capacitors to prevent damage to the crowbar due to overload.

To analyze RF protection under scenarios I and II, the circuit shown in Fig. 25 is simulated. Several RF bunkers composed of a decoupling reactor and a filtering capacitor are connected to the same dc bus. A resistor is connected in series with each capacitor to limit the fault current. The crowbar has an operation time of less than 1 μs in the event of a short circuit.

The protection sequence for an RF fault caused by klystron arcing under Scenario I is illustrated in Fig. 26. At time $t = 1.5$ s, a klystron arcing fault is detected, triggering the crowbar in the faulty RF bunker. Consequently, the dc voltage immediately drops, causing the filtering capacitors in the other RF bunkers to discharge with oscillatory behavior due to the decoupling inductances. The fault current is limited by the decoupling reactors and the series resistance in the bunkers. In response to the fault, the rectifier inverts its polarity, preventing any contribution from the ac network and enabling

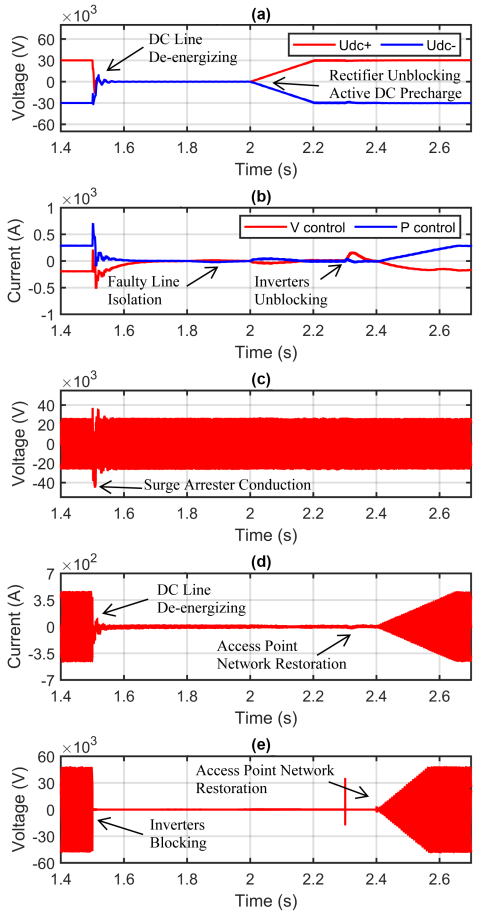

FIGURE 24. Pole-to-ground protection sequence when using hybrid converters. (a) DC voltage measured at the rectifier terminals. (b) DC current measured at the rectifier terminals. (c) AC voltage of the rectifier stations. (d) AC current of one of the rectifier stations. (e) Voltage at one of the medium voltage access point networks.

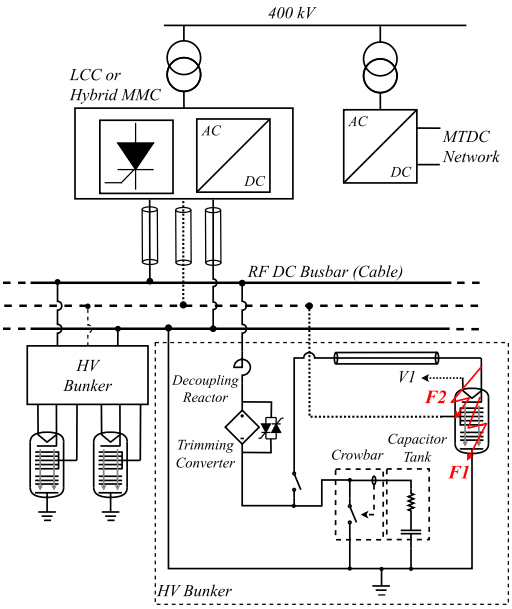

FIGURE 25. Circuit used to study RF protection under scenarios I and II. The fault happens between the high-voltage terminal of the klystron and ground. A bypassing thyristor is added across the trimming converter to protect it from overcurrent.

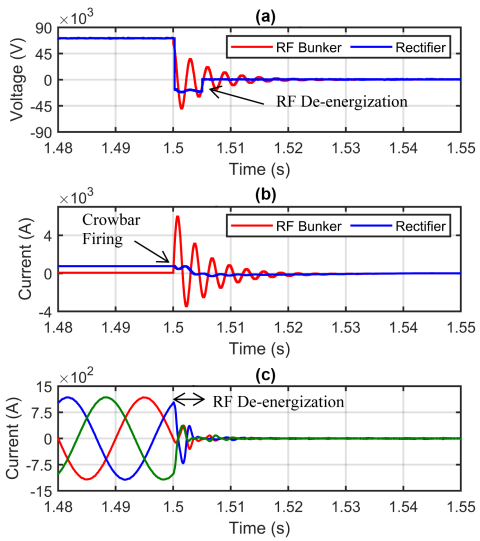

FIGURE 26. DC short-circuit resulting from the crowbar triggering when hybrid MMC converters are used. (a) DC voltage measured at the rectifier terminals and at the RF bunker input. (b) DC current measured at the rectifier terminals and at the RF bunker input. (c) AC current of the rectifier station.

the discharge of the stored energy. From the ac network's perspective, the fault does not cause any overcurrent, and the converter is still available for providing ancillary services. Note also that if the fault occurs between the other two terminals available in the klystron (F2 in Fig. 25), the protection principle would be the same.

In a similar way, when a thyristor converter is used in the RF network, the dc network is de-energized by switching the converter into inverting mode. The simulation results of this protection method are presented in Fig. 27. It is important in this case to ensure that the rectifier supplying the MTDC network remains stable during the transient caused by forcing RF station into inversion mode.Fig. 27(d) shows the ac currents injected by the MMC into the 400 kV network. As depicted, when the *LCC* starts the fault-clearing sequence and current is brought to zero, the MMC stops compensating for harmonics and reactive power but continues to operate normally and supply the MTDC network.

Finally, although not depicted here, the restoration sequence would be started after arc extinction or isolation of the faulty circuit. The restoration would be done by ramping-up the dc voltage as already shown.

C. PROTECTION UNDER SCENARIO III

The use of a three-terminal MMC for simultaneous supply of the RF system and the MTDC network requires special attention to protection. The converter is assumed to have a hybrid structure with enough full-bridge submodules to produce zero output voltage in the event of a fault. Three main

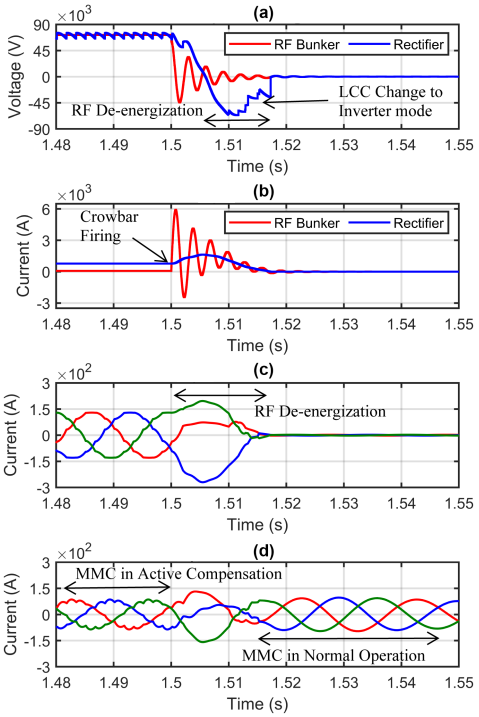

FIGURE 27. **DC short-circuit resulting from the crowbar triggering when *LCC* converters are used. (a) DC voltage measured at the rectifier terminals and at the RF bunker input. (b) DC current measured at the rectifier terminals and at the RF bunker input. (c) AC current of the rectifier station. (d) AC currents of the MTDC MMC.**

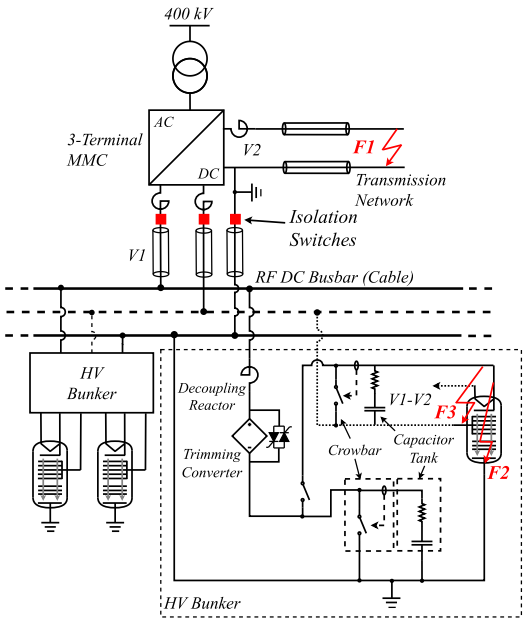

FIGURE 28. **Circuit used to study RF protection under scenario III.**

fault scenarios are analyzed based on the diagram shown in Fig. 28. As mentioned, grounding one pole is necessary in a three-terminal MMC, so both pole-to-pole and pole-to-ground faults will result in overcurrents.

The protection sequence for an MTDC network fault is illustrated in Fig. 29. When a fault occurs at time $t = 1.5$ s, the priority is to clear and isolate the fault to resume normal operation. The converter is switched to dc current control mode, reducing the fault current to zero. This enables the faulty line to be isolated, and at $t = 2$ s, the MTDC voltage and inverter stations can be restored. The inverter stations are fully operational again at $t = 2.3$ s. In a similar manner, the RF power is restored at $t = 2.4$ s. Throughout the entire process, the converter remains controllable. The proposed control strategy guarantees the energy balancing of the converter arms during normal and fault conditions as can be seen in Fig. 29(d).

In the case of the fault denoted as F2 in Fig. 28, a similar behavior is expected, except for the application of negative dc voltage for de-energization. The isolation of the fault can be done for the whole RF network at converter terminals or at the level of the RF bunker. The priority is given to MTDC network restoration.

If the short circuit involves the top and middle terminals, only the V_1–V_2 voltage is compromised. The protection sequence in this case is shown in Fig. 30. As already explained, the RF fault requires de-energizing the affected part of the

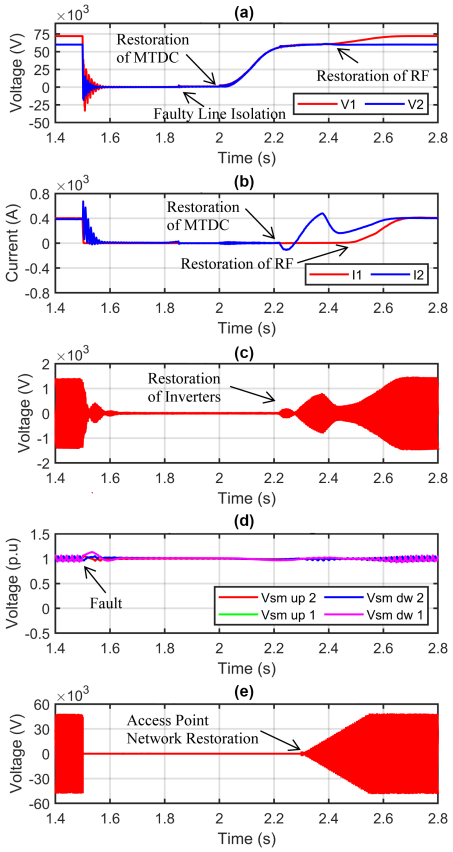

FIGURE 29. **Fault-clearing sequence when fault happens at the MTDC network. (a) DC voltages measured at the rectifier top and middle terminals. (b) DC currents measured at the rectifier top and middle terminals (c) AC current of the rectifier stations. (d) Average submodule voltages of the four arms of the 3 T MMC. (e) Voltage at one of the medium voltage access point networks.**

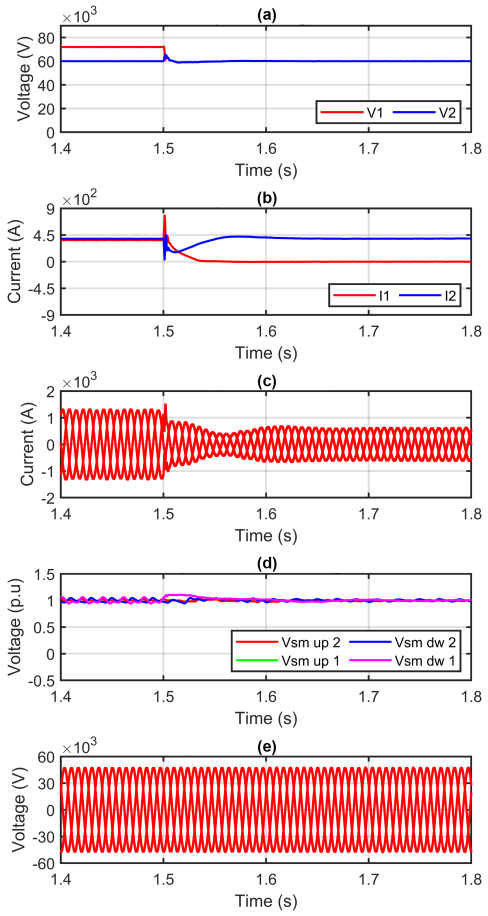

FIGURE 30. Fault-clearing sequence when fault happens between the top and the middle terminal of the 3 T MMC. (a) DC voltages measured at the rectifier top and middle terminals. (b) DC currents measured at the rectifier top and middle terminals (c) AC current of the rectifier stations. (d) Average submodule voltages of the four arms of the 3 T MMC. (e) Voltage at one of the medium voltage access point networks.

network. However, in this case, the supply of the MTDC network is not affected, and only minor perturbation of the dc voltage is expected due to the coupling that exists between the terminals due to the dc reactors. Once again, the proposed strategy manages to keep the arm voltages balanced and the converter supplying the MTDC network. The resulting transient is not transferred to the access point networks, as shown in Fig. 30(e).

VI. CONCLUSION

This article has analyzed the technical feasibility of three different alternatives for the dc-powering of the FCC, namely, the following.

1) *Scenario I:* The RF system and the dc transmission network are powered by separate power converters.
2) *Scenario II:* Use of *LCC* to provide power to the RF system, while the converter supplying the dc network compensates for *LCC* reactive power and harmonics.
3) *Scenario III:* A three-terminal converter powers the dc-grid and RF systems simultaneously.

The three topologies have been subject to extensive studies, both during normal operation and in fault conditions. In Scenario I, the installation of two converters increases the system's footprint. However, it enables independent operation of the two subsystems, resulting in higher reliability compared to Scenarios II and III, where the systems are interconnected. The symmetric monopole configuration has been identified as the most suitable scheme for constructing the transmission network, and a thorough analysis has been conducted to ensure adequate protection measures.

AC breakers have been determined to be a suitable solution for protecting the transmission network in Scenario I. However, in the event of a pole-to-ground fault, it is necessary to discharge the MTDC network before restoration to prevent overvoltage on the healthy pole. The use of hybrid converters has also been explored for powering the RF systems, as they have the capability to regulate the dc voltage, which is a requirement of the RF system. It has been demonstrated that including an adequate number of full-bridge submodules allows the converter to effectively handle a dc fault, whether it occurs accidentally or is triggered by the crowbar.

In Scenario II, on the other hand, there is potential for additional optimization in terms of space requirements and efficiency. Thyristor converters have been identified as suitable for operation alongside MMCs, as the MMCs can handle reactive power and harmonic compensation. These thyristor converters offer robust dc voltage control and fault-handling capacity, making them advantageous choices for powering the RF systems. Furthermore, it has been verified that the MMC control can ride-through a fault in the RF system without impacting power transmission along the MTDC network.

It has also been verified that thyristor converters are efficient in de-energizing the RF network by reducing the energy discharged into the crowbar. This is achieved by applying a negative output voltage when a fault is detected. The same principle, in the case of the MMC, would require the addition of more full-bridge submodules to achieve the negative voltage.

Finally, Scenario III proposes a three-terminal MMC to simultaneously power the RF system and the MTDC network. An energy control scheme based on the injection of 50 Hz and 100 Hz circulating currents allows stable operation of the MMC under various operating conditions. The control has been proven effective in the event of MTDC or RF faults, with the converter remaining stable and allowing the network to be restored once the fault has been cleared. This converter offers a more compact solution, but reliability could be negatively impacted, especially in the event of frequent RF arcing.

These conclusions underscore the feasibility of using dc networks to power the FCC, positioning this approach as a viable powering option when evaluating the feasibility and cost of the machine. Of the three strategies analyzed, the three-terminal MMC emerges as particularly promising when tasked with performing both proposed functions simultaneously. It offers a significant reduction in footprint compared

to the other two solutions. Consequently, further research and development will focus on this topology.

REFERENCES

[1] M. Mangano et al., "FCC physics opportunities: Future circular collider conceptual design report volume 1," Future Circular Collider, (CERN), Dec. 14, 2018. [Online]. Available: https://cds.cern.ch/record/2651294

[2] H. Wang and M. Redfern, "The advantages and disadvantages of using HVDC to interconnect AC networks," in *Proc. 45th Int. Universities Power Eng. Conf.*, 2010, pp. 1–5.

[3] S. Kolluri, P. Thummala, R. Sapkota, S. K. Panda, and D. Rendusara, "Subsea power transmission cable modelling: Reactive power compensation and transient response studies," in *Proc. IEEE 17th Workshop Control Model. Power Electron.*, 2016, pp. 1–6.

[4] H. Alafnan, "Fault analysis and protection solution for DC transmission lines of solar farms using superconducting fault current limiters," in *Proc. 5th Int. Conf. Power Electron. Their Appl.*, 2022, 1–5.

[5] L. Barthold, R. Adapa, H. Clark, and D. Woodford, "System advantages in conversion of AC transmission lines to DC," in *Proc. 9th IET Int. Conf. AC DC Power Transmiss.*, 2010, pp. 1–5.

[6] J. Yu, K. Smith, M. Urizarbarrena, N. MacLeod, R. Bryans, and A. Moon, "Initial designs for the ANGLE DC project; converting existing AC cable and overhead line into DC operation," in *Proc. 13th IET Int. Conf. AC DC Power Transmiss.*, 2017, pp. 1–6.

[7] G. Radman, A. Pama, J. Powell, and D. Gao, "Dynamic voltage stability improvement using coordinated control of dynamic VAR-sources," in *Proc. IREP Symp.-Bulk Power Syst. Dyn. Control—VII. Revitalizing Oper. Rel.*, 2007, pp. 1–6.

[8] M. Colmenero, F. Blanquez, and K. Kahle, "Transient voltage dip mitigation system based on hybrid modular multilevel converters," in *Proc. 22nd Eur. Conf. Power Electron. Appl.*, 2020, pp. P.1–P.10.

[9] A. Lesnicar and R. Marquardt, "An innovative modular multilevel converter topology suitable for a wide power range," in *Proc. IEEE Bologna Power Tech Conf. Proc.*, 2003, pp. 6–pp.

[10] S. Debnath, J. Qin, B. Bahrani, M. Saeedifard, and P. Barbosa, "Operation, control, and applications of the modular multilevel converter: A review," *IEEE Trans. Power Electron.*, vol. 30, no. 1, pp. 37–53, Jan. 2015.

[11] M. C. Moratalla, R. Vidal-Albalate, F. R. B. Delgado, and R. Blasco-Gimenez, "Fault-tolerant strategies in MMC-based high power magnet supply for particle accelerator," *Math. Comput. Simul.*, 2023, doi: 10.1016/j.matcom.2023.07.014

[12] O. E. Oni, I. E. Davidson, and K. N. I. Mbangula, "A review of LCC-HVDC and VSC-HVDC technologies and applications," in *Proc. IEEE 16th Int. Conf. Environ. Elect. Eng.*, 2016, pp. 1–7.

[13] A. Farghly, M. El Habrouk, K. Ahmed, A. Abdel-khalik, and R. Hamdy, "Active power filter for12-pulse LCC converter employed in LCC-MMC hybrid HVDC system," in *Proc. 23rd Int. Middle East Power Syst. Conf.*, 2022, pp. 1–7.

[14] C. Martins, F. Bordry, and G. Simonet, "A solid state 100 kV long pulse generator for klystrons power supply," in *Proc. 13th Eur. Conf. Power Electron. Appl.*, 2009, pp. 1–10.

[15] R. Vidal-Albalate, D. Soto-Sanchez, E. Belenguer, R. Peña, and R. Blasco-Gimenez, "Modular multi-level DC-DC converter for high-power and high-voltage applications," in *Proc. 41st Annu. Conf. IEEE Ind. Electron. Soc.*, 2015, pp. 003798–003803.

[16] V. Teryaev, S. Shchelkunov, and J. Hirshfield, "Innovative two-stage multibeam klystron: Concept and modeling," *IEEE Trans. Electron Devices*, vol. 67, no. 7, pp. 2896–2899, Jul. 2020.

[17] V. Teryaev, S. Shchelkunov, and J. Hirshfield, "90% efficient two-stage multibeam klystron: Modeling and design study," *IEEE Trans. Electron Devices*, vol. 67, no. 12, pp. 5777–5782, Dec. 2020.

[18] F. Bordry and H. Thiesen, "LHC inner triplet powering strategy," in *Proc. Part. Accel. Conf.*, 2001, vol. 1, pp. 633–635.

[19] X. Zhang, G. Gao, P. Fu, Z. Song, and B. Wang, "Design a suitable test scheme for triggering bypass protection test of ITER PF converter unit," *IEEE Trans. Plasma Sci.*, vol. 46, no. 5, pp. 1318–1322, May 2018.

[20] D. Aguglia,, "Interconnected High-voltage pulsed-power converters system design for H- ion sources," *IEEE Trans. Plasma Sci.*, vol. 42, no. 10, pp. 3070–3076, Oct. 2014.

[21] J. Jensen and W. Merz, "Light triggered thyristor crowbar for klystron protection application," in *Proc. Part. Accel. Conf.*, 2003, vol. 2, pp. 749–751.

[22] O. Brunner, H. Frischholz, and D. Valuch, "RF power generation in LHC," in *Proc. Part. Accel. Conf.*, 2003, vol. 1, pp. 473–475.

[23] W. Wang and M. Barnes, "Power flow algorithms for multi-terminal VSC-HVDC with droop control," *IEEE Trans. Power Syst.*, vol. 29, no. 4, pp. 1721–1730, Jul. 2014.

[24] R. Chai, B. Zhang, Z. Hao, T. Zheng, S. Ma, and D. Chen, "Control strategies of MMC-HVDC connected to passive networks," in *Proc. IEEE Int. Conf. IEEE Region*, 2013, vol. 10, pp. 1–4.

[25] Y. Chen et al., "Analysis of transfer operation between metallic and ground return configurations for multi-terminal HVDC systems," in *Proc. IEEE 4th Workshop On Electron. Grid*, 2019, pp. 1–5.

[26] Y. Luo et al., "Analytical calculation of transient short-circuit currents for MMC-Based MTDC grids," *IEEE Trans. Ind. Electron.*, vol. 69, no. 7, pp. 7500–7511, Jul. 2022.

[27] A. Bertinato, P. Torwelle, G. Dantas De Freitas, M. Colmenero, and B. Raison, "Pole-to-ground fault protection strategy for HVDC grids under symmetrical monopolar configuration," in *Proc. IEEE Milan PowerTech*, 2019, pp. 1–6.

[28] W. Leterme, P. Tielens, S. De Boeck, and D. V Hertem, "Overview of grounding and configuration options for meshed HVDC grids," *IEEE Trans. Power Del.*, vol. 29, no. 6, pp. 2467–2475, Dec. 2014.

[29] Z. He, P. Zeng, and J. Liu, "Transient modeling and fault current calculation of hybrid MMC when riding through DC-side pole-to-ground fault," in *Proc. IEEE Power Energy Soc. Gen. Meeting*, 2021, pp. 01–05.

[30] M. Wang, J. Beerten, and D. V. Hertem, "Pole voltage balancing in HVDC systems: Analysis and technology options," in *Proc. IEEE Milan PowerTech*, 2019, pp. 1–6.

[31] M. Bucher and C. Franck, "Comparison of fault currents in multiterminal HVDC grids with different grounding schemes," in *Proc. IEEE PES Gen. Meeting—Conf. Expo.*, 2014, pp. 1–5.

[32] G. Guo et al., "HB and FB MMC based onshore converter in series-connected offshore wind farm," *IEEE Trans. Power Electron.*, vol. 35, no. 3, pp. 2646–2658, Mar. 2020.

[33] R. Zeng, L. Xu, L. Yao, and B. Williams, "Design and operation of a hybrid modular multilevel converter," *IEEE Trans. Power Electron.*, vol. 30, no. 3, pp. 1137–1146, Mar. 2015.

[34] R. Zeng, L. Xu, L. Yao, and D. Morrow, "Precharging and DC fault ride-through of hybrid MMC-Based HVDC systems," *IEEE Trans. Power Del.*, vol. 30, no. 3, pp. 1298–1306, Jun. 2015.

[35] H. Dingwen, W. Li, Z. Lincui, and A. Le, "Design and application of distributed energy dissipation device in LCC-MMC transmission system," in *Proc. 16th IET Int. Conf. AC DC Power Transmiss.*, 2020, pp. 2329–2334.

[36] Y. Ma, H. Li, G. Wang, and J. Wu, "Fault analysis and traveling-wave-based protection scheme for double-circuit LCC-HVDC transmission lines with shared towers," *IEEE Trans. Power Del.*, vol. 33, no. 3, pp. 1479–1488, Jun. 2018.

[37] C. Batard, M. Machmoum, F. Alvarez, and P. Ladoux, "Control of shunt active power filter for railway sub-station," in *Proc. 32nd Annu. Conf. IEEE Ind. Electron.*, 2006, pp. 2511–2516.

[38] Y. Li and F. Wang, "Arm inductance selection principle for modular multilevel converters with circulating current suppressing control," in *Proc. 28th Annu. IEEE Appl. Power Electron. Conf. Expo.*, 2013, pp. 1321–1325.